Plasma Physics and Controlled Fusion Vol.28, No.1A pp.71-83, 1986 0741-3335/86$3.00+ .00
Printed in Great Britain

ION CYCLOTRON RESONANCE HEATING ON TEXTOR

A.M. Messiaen+, V.P. Bhatnagar, T. Delvigne, P. Descamps, F. Durodié, M. Jadoul, R. Koch, D. Lebeau, D.I.C. Pearson, P.E. Vandenplas, A. Vanderstraeten, R. Van Nieuwenhove, G. Van Oost, G. Van Wassenhove, R.R. Weynants+

Laboratoire de Physique des Plasmas - Laboratorium voor Plasmafysica
Association "Euratom-Etat belge" - Associatie "Euratom-Belgische Staat"
Ecole Royale Militaire - B 1040 Brussels - Koninklijke Militaire School
and
H.L. Bay, G. Bertschinger, W. Bieger, P. Bogen, G.A. Campbell[1], R.W. Conn[1], K.H. Dippel, H.G. Esser, K.H. Finken, G. Fuchs, B. Giesen, D.M. Goebel, R. Graffmann, S.E. Guthrie[2], H. Hartwig, E. Hintz, G. Hrehuss[3], F. Hoenen, K. Hoethker, A. Kaleck, L. Könen, M. Korten, Y.T. Lie, K. Liung[1], M. Lochter, A.E. Pontau[2], A. Pospieszczyk, D. Rusbüldt, U. Samm, B. Schweer, J. Schlüter, H. Soltwisch, G. Thomas[2], F. Waelbroeck, G. Waidmann, P. Wienhold, J. Winter, G.H. Wolf

Institut für Plasmaphysik, Kernforschungsanlage Jülich GmbH, Association "Euratom-KFA", D-5170 Jülich, FRG

ABSTRACT

Ion cyclotron heating on TEXTOR has now reached the Megajoule level, The heating scenario is normally mode conversion but occasionally minority heating in a D-(H) plasma. With appropriate wall conditioning by carbonization more than 1 MW of RF power has been injected for long pulse durations (~ 1 s). The ICRF heated plasma is characterized by a quasi-stationarity of all plasma parameters, little if no impurity increase and a loop voltage reduction resulting in the total power coupled to the plasma reaching six times the remaining ohmic power input. Evidence of the coupling of the RF power to the plasma is obtained from the increase of the thermal load on the limiters and central energy deposition is supported from analysis of the sawtooth heating rate. The energy deposition profile appears to be broader than in the OH case. A detailed study of the global energy confinement time shows a degradation with additional RF heating which is found to scale with the power and the plasma parameters as in the case of neutral beam heating experiments performed in the L-mode regime with gettered walls.

KEYWORDS

Long pulse ICRH ; tokamak ; impurity ; carbonization ; confinement ; energy deposition ; sawteeth analysis ; scaling ; coupling.

1. INTRODUCTION

ICRF heating on TEXTOR has been carried out at the MW power level for long pulse, low impurity plasma conditions. The confinement properties of the discharge going from the pure OH regime to the case dominated by additional heating have been studied in detail.

The TEXTOR ICRH system consists of two independent power lines, each being fed by a transmitter able to generate 3 second, 1.5 MW pulses in the frequency range 25-29 MHz [1]. Each line is connected on the low field side, near the equatorial plane, to two $\lambda/4$ stainless steel strip line antennae which, as shown on Fig. 1a, are placed along the heated liner of TEXTOR in the same azimuthal plane and completely surround the plasma. The two antennae, of which a transverse cut is shown on Fig. 1b, differ only in the width of the central conductor which is narrower for the top antenna. The electrostatic screen resembles a venetian blind with blades aligned in the direction of the total magnetic field for $q_a = 3$.

Normal TEXTOR machine parameters are $B_t = 2T$, $R_o = 1.75$ m, with plasma current $I_p < 460$ kA

+ Senior research associate at the NFSR, Belgium. [1]University of California at Los Angeles, U.S.A. [2]Sandia National Laboratories, Livermore, U.S.A. [3]Central Research Inst. of Physics, Budapest, Hungary.

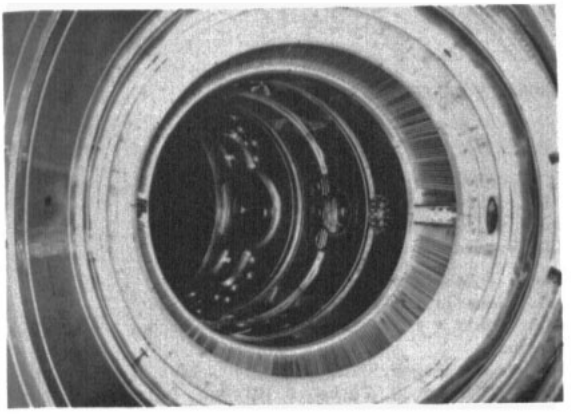

Fig. 1a. View of the TEXTOR ICRH antennae.

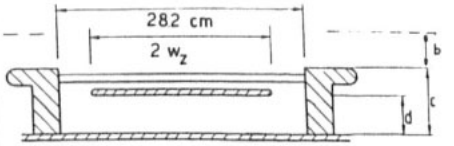

Fig. 1b. Cross section of an antenna with its central conductor, side limiters and electrostatic shield. The dotted line corresponds to the usual main limiter radius a = 46 cm. Mean distances in cm : d = 3.85, c = 6.94, b = 2.8, $2w_z$ = 20.5 (bottom antenna) or 7.0 (top antenna).

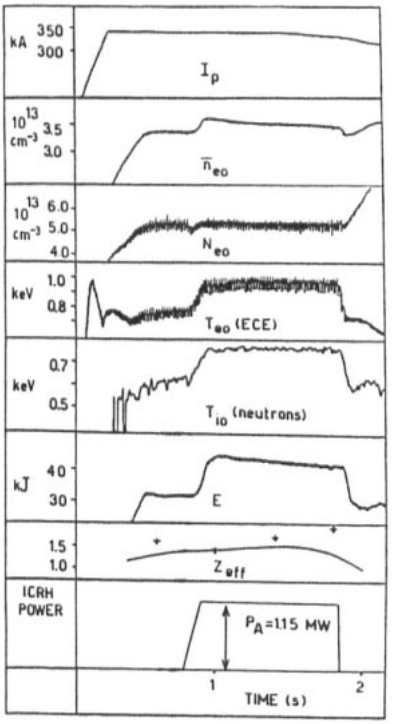

Fig. 2a. Evolution versus time of plasma current I_p, central line density n_{eo}, central density N_{eo}, central electron and ion temperatures T_{eo} and T_{io}, plasma energy content E, central Z_{eff} (solid line : from Spitzer resistivity and q_o = 1 ; crosses : from soft X-rays) and RF power P_A for the shot 14169.

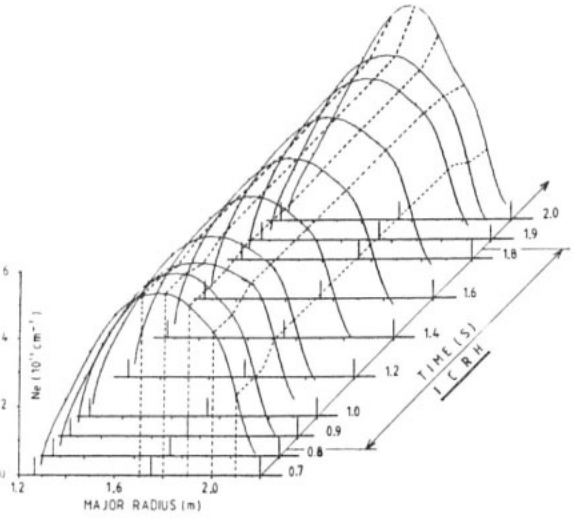

Fig. 2b. Evolution of the density profile (averaged over the sawtooth period) as a function of time for the shot 14169.

and central average line density $\bar{n}_{eo} < 5.3 \times 10^{13} cm^{-3}$ in a D-(H) plasma with hydrogen concentration ranging from < 1 % to ∿ 25 % . The machine was operated normally with the main stainless steel limiters at a = 46 cm but the pump limiter ALT-1 [2] with a graphite head has also been used as main limiter without a significant change in the results. As the antenna current antinode lies on the high field side of the machine, about 80 % of the radiated power is launched from this side. When the hydrogen concentration is sufficiently large (> 1.5 %) the heating scenario will be predominantly the mode conversion one for which the wave launched from the HFS is partly converted into an electrostatic wave at a confluence layer whose location is given approximately by the relation $R-R_o = R_o \{ \frac{\omega_{CH}(R_o)}{\omega} (\frac{1 - X_H/2}{1 + X_H})^{1/2} - 1 \}$. In this formula R_o is the main radius, $\omega_{CH}(R_o)$ the hydrogen cyclotron frequency at $R = R_o$ and $X_H = N_H/(N_H+N_D)$ is the isotope ratio in the plasma with hydrogen and deuterium densities respectively given by N_H and N_D . Direct minority heating near the $\omega = \omega_{CH}(R)$ layer by the fast wave (or even the slow wave [3]) transmitted through the confluence or launched from the LFS can also occur. Experiments in a pure minority heating regime with X_H < 1 % have also been carried out. The results presented in this paper have been partly summarized in reference [4].

2. LOW IMPURITY, LONG PULSE ICRH WITH CARBONIZED WALLS

2.a. Wall Conditioning.

An essential feature for the successful application of ICRH on TEXTOR is a proper conditioning of the machine by wall carbonization. As reported previously [5], prior to the application of this procedure, the edge plasma and the scrape-off layer were profoundly perturbed by the RF pulse. The maximum RF power was limited by plasma disruption occurring after a shrinking of the discharge, to about 200 kW applied for a maximum of 100 ms. The OH discharges in Deuterium were characterized by a rather large Z_{eff} (> 3).

A strong modification of the plasma-surface interaction is obtained by the deposition of about 300 monolayers of carbon over all the inner surfaces by means of glow discharge in a mixture of D_2 and CH_4 [6]. The level of radiation from heavy impurities in tokamak discharges then decreases at least by one order of magnitude ; the level of oxygen radiation is also strongly reduced. Consequently, the part of the input power retrieved on the limiter increases (e.g. thermal load on ALT increased by a factor 1.5 at $\bar{n}_{e\,o} = 3 \times 10^{13} cm^{-3}$) and the radiation seen by bolometry is reduced. The deposited layers are dense hydrogenated amorphous carbon films and show good adhesion on stainless steel and inconel. Due to the strongly increased recycling of the carbonized wall, the H/D isotopic ratio in the discharge is very dependent on that existing in the carbon layer. A special type of procedure where carbonization periods alternate with glow discharges in pure D_2 has been developed in order to reduce, by isotope exchange, the H content with respect to the D content of the deposited layers [6]. With such a procedure, an isotopic ratio X_H of typically 3-5 % in the discharge is achievable. For the very low-values of X_H < 1 % necessary for pure minority heating carbonization in a mixture of D_2 and CD_4 has been successfully carried out.

By conditioning in this manner, the total input power to the antennae has now been taken up to 1.3 MW and the total input energy up to 1.4 MJ, the limitation being the voltage stand-off (see discussion in section 3). Note that with a non-optimized carbonization procedure or in the presence of injected impurities or leaks, the maximum power can again become limited by plasma disruption [5].

2.b. Low-Impurity Long-Pulse ICRH.

Fig. 2 shows the time evolution of various parameters for a typical long pulse of RF energy above 1 MJ. The stationarity of the plasma conditions is manifest during the ICRH pulse.

(i) Density. Typical time evolutions of the electron density profile (averaged over the sawtooth period) are shown in Fig. 2a from the Abel inverted HCN interferometric data and in Fig. 3 from the evolution of the density profile parameter α_n . This parameter describes the density profile by an approximate law : $N_e \propto 1 - (r/a)^{\alpha_n}$ [7]. The density profile broadens at the beginning of the ICRH pulse and afterwards remains practically unchanged. An increase of central line density always accompanies the RF pulse (see Fig. 2a). It is partly due to the profile broadening and its magnitude is, even in absolute value, more pronounced at low densities. It depends also on the machine conditioning and the plasma current. Without making any attempt to reach the density limit, a Murakami factor $\bar{n}_{Mu} = \bar{n}_{eo}(10^{13} cm^{-3}) R(m)$ $q_a/B_t(T)$ of 1.25 has been obtained during stable ICRH pulses.

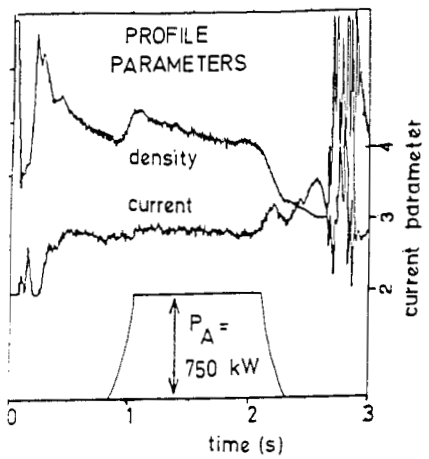

Fig. 3. Density profile parameter α_n and current density profile parameter α_j together with the RF power pulse shown versus time for the shot 15331.

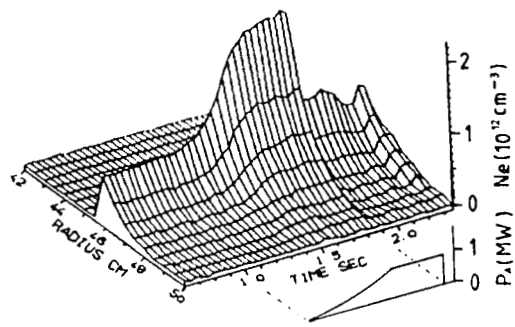

Fig. 4. Edge density profile versus time for the shot 13704 measured with the Li-atom beam technique [5]. The RF pulse is also shown. The main limiter radius is 44 cm.

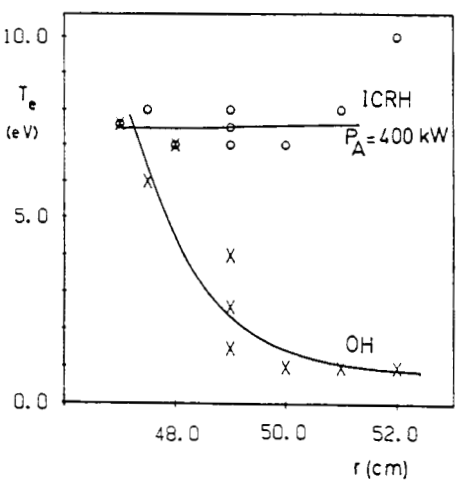

Fig. 5a. Electron temperature measured by Langmuir probes in the SOL during OH and ICRH portions of the discharge, as a function of the minor radius (a = 46 cm, r_{wall} = 52.5cm).

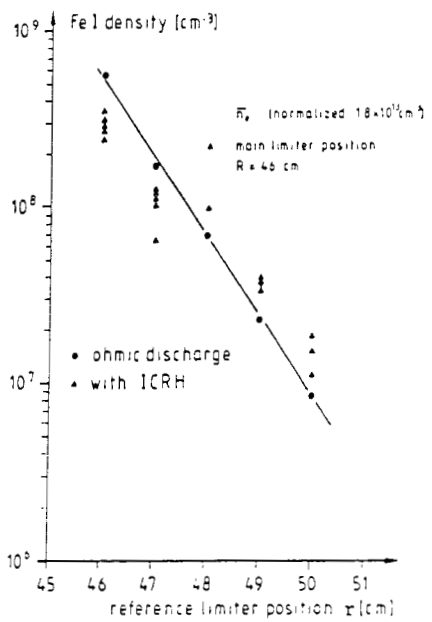

Fig. 5b. Iron neutral density observed, in the SOL, in front of a movable limiter measured by means of laser induced fluorescence for the same series of shots as in Fig. 5a), during OH and ICRH.

Rather large sawtooth density oscillations are seen in the $q < 1$ region (e.g. $r \lesssim 12$ cm for $I_p = 340$ kA). A typical display of the central electron density N_{eo} as obtained from Abel inversion with a high temporal resolution is shown on Fig. 2a.

The relative density change is largest in the plasma edge and in the scrape-off layer (SOL). As shown on Fig. 4, the doubling seen by the interferometer is confirmed by a Lithium beam probe [8] which furthermore indicates an increase of the density decay length (e.g. from 0.7 to 1.0 cm in the case of Fig. 4). These last results are corroborated by Langmuir probe measurements which also show that the density near the wall ($r = 52.5$ cm) increases (e.g. in the case of $a = 46$ cm from about 10^{10}cm^{-3}in OH it increases by a factor ~ 4).

The results reported here differ strongly from those described in [5] prior to wall carbonization.

(ii) Temperature, loop voltage and current density profile. Electron heating over the whole profile is observed by Thomson scattering and soft X-rays (see Fig. 2 of Ref. [4]) and from ECE measurements for the $r < 17$ cm part of the profile (see Fig. 2 of Ref. [8]).Significant sawtooth activity is always observed during ICRH as seen on the central T_{eo} measured by ECE in Fig. 2a ; this is specifically discussed in section 4.2.

Two observations are in agreement with the fact that the T_e profile, averaged on the sawtooth period denoted $< T_e(r) >$, does not appreciably change during ICRH : 1°) the current density profile J(r) measured by a HCN polarimeter shows either no change or at most a slight flattening during the RF pulse. Fig. 3 shows a typical evolution of the current density factor α_j during a shot with a long RF pulse. The factor α_j expresses the current profile by the approximate relation $J = J_o(R_o/R)[(1 - r^2/a^2)^{\alpha_j} - [(R - R_o)/R]\ \varepsilon(r)]$ where $\varepsilon(r) < 0.5$ is a correction factor [7]. No significant change in α_j is seen during ICRH, in contrast to the behaviour of the density profile factor α_n. In TEXTOR, it has been verified that J(r) is linked to $<T_e(r)>$ by the Spitzer resistivity [9] ; 2°) the loop voltage V_l always shows a decrease during ICRH, e.g. from ~ 1 V in OH down to ~ 0.7 V for a 1 MW ICRH shot, which is roughly consistent with the observed increase of T_{eo}.

Measurements of electron temperature in the SOL and near the plasma edge indicate an increase during ICRH near the wall. Nearer the edge of the plasma this temperature increase becomes smaller and in some cases a decrease has even been observed. Fig. 5a shows a typical T_e behaviour in the SOL during OH and ICRH as measured by a Langmuir double probe. Fig. 5b shows the neutral iron density versus the minor radius observed by laser induced fluorescence [10] in front of a movable limiter displaced in the SOL. An increase of neutral Fe density during ICRH due to the T_e increase is indeed observed far out in the SOL, whereas a decrease of neutral Fe density is seen at small distances (< 1.5 cm) from the main limiter radius (46 cm) which can only been explained by a T_e decrease. It should be noted that the Fe sputtering measurement was only possible with mild wall carbonization since the Fe concentration becomes too low for standard carbonization.

No ion temperature profile measurement is available. The central ion temperature T_{io} has been deduced from the neutron count rate. It has been checked that for plasma conditions used for the ICRH experiments the neutrons are only of thermonuclear origin. The obtained values are consistent with the results of charge-exchange measurements performed only at low densities. During the OH phase the behaviour of the central ion temperature is well described by an Artsimovitch law : $T_{io}\, f^{-1/3} = 2.76 \times 10^{-6}(\bar{n}_{eo} R_o^2 I_p B_t)^{1/3}$ (eV, MKSA units ; $f = x^{1/2}(1 - x)$; $x = T_{io}/T_{eo}$; deuterium). With ICRH, an ion temperature increase partly due to the transfer of energy between electrons and ions and partly to the direct coupling of RF power to the ions (see section 4.2) is observed.

The electron and ion temperature increases achieved during ICRH depend on the density and the confinement properties during heating whose dependence on the discharge conditions is discussed in detail in section 5. As seen on Fig. 6, for a central chord density $\bar{n}_{eo} \simeq 3.5 \times 10^{13}$cm^{-3} and for $I_p = 340$ kA and $B_t = 2$ T we observe a heating efficiency $\bar{n}_{eo}\Delta T_o/P_{RF} \simeq 1.1$ eV $\times 10^{13}$cm^{-3}/kW for electrons and $\simeq 0.7$ eV $\times 10^{13}$cm^{-3}/kW for ions. These values are in agreement with the measured increase of the plasma energy content E at this density (see section 5). Also indicated in Fig. 6 are the predictions of the abovementioned Artsimovitch law, i.e. the expected T_{io} increase due only to the T_{eo} increase through equipartition without any RF power directly absorbed by the ions (see discussion in section 4.2).

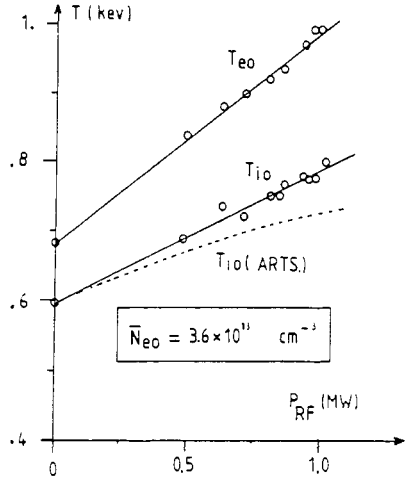

Fig. 6. Dependence of T_{eo} and T_{io} on P_{RF} at a constant central line density $\bar{n}_{eo} = 3.6 \times 10^{13} cm^{-3}$. The dotted line gives the evolution of the Artsimovitch law value due to its T_{eo} dependence.

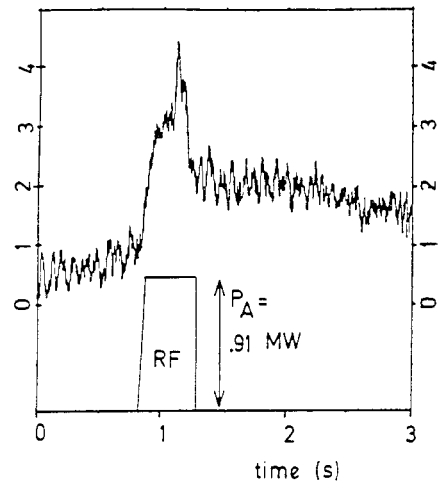

Fig. 7. Radiated power flux observed by a bolometer and RF power versus time during the shot 14725. Before ICRH, P_{OH} = 340 kW and during ICRH, P_{tot} = 1.06 MW.

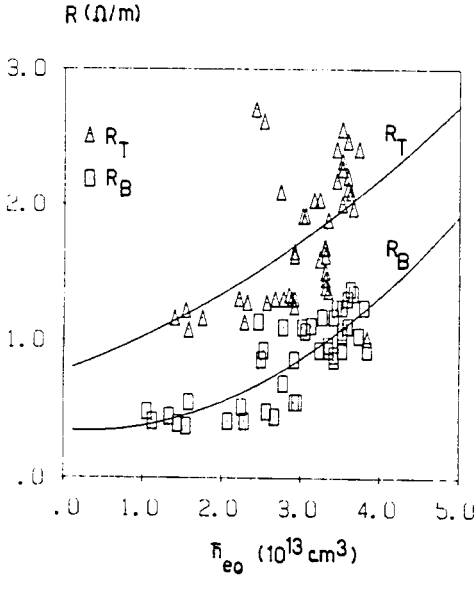

Fig. 8. Evolution versus the central chord density $\bar{n}_{eo}$ of the experimental values of the specific loading resistances R_T and R_B from data collected over many days of operation with a = 46 cm and F = 27 MHz. The solid lines correspond to the best parabolic fit.

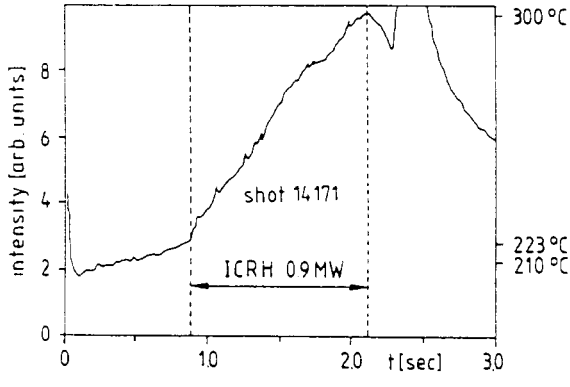

Fig. 9. Evolution versus time of the infrared radiation from the test limiter surface during the shot 14171. The heat load increases by a factor 3.9 during ICRH with respect to OH whereas P_{tot} rises by a factor 3.1 (from 335 kW during OH to 1.03 MW during ICRH).

(iii) Energy content. The plasma energy content E is directly measured by diamagnetism. This measurement is confirmed by NT-profile integration (assuming identical profiles for electron and ion temperatures) and by $\beta_p + l_i/2$ measurements. The errorbar on E is estimated to be about ± 20 %. The dependence of E on the discharge parameters is further discussed in sections 4 and 5.

(iv) Impurities. As seen from the behaviour of the brilliance of impurities lines (see Fig. 1 of Ref. [4]), low Z and metallic impurities attain stationary conditions very rapidly. As indicated in Table I, the central carbon concentration inferred from continuum radiation in these carbonized discharges is below 2 to 3 % and does not increase during RF. This is also confirmed by the brilliance of C_V which changes nearly in proportion to the edge density. The sum of the central metallic impurity concentrations (Fe, Cr, Ni) measured by X ray spectroscopy in the OH discharge ranges from 10^{-5} to 10^{-4}. A roughly constant increment of $(6 \pm 2) \times 10^{-5}$ is observed when 1 MW of RF power is injected. This results in the low-value Z_{eff} obtained either from the soft X-ray measurements or, for the on-axis values, from Spitzer resistivity with the assumption that $q_o \gtrsim 1$. As seen on Fig. 2a the low Z_{eff} remains stationary during a long ICRH pulse.

time window (s)	r (cm)	concentration of C or O %	Cr %	Fe %	Ni %	Z_{eff} C	Z_{eff} or O
0.4-0.8	5	1.98	0.48 .000	.000	-	1.6	1.3
(OH)	15	2.19	0.47 .001	.000	.001	1.7	1.3
0.8-1.2	5	1.42	0.41 .001	.002	.001	1.4	1.2
(ICRH)	15	2.02	0.50 .001	.002	.001	1.6	1.3
1.2-1.6	5	2.13	0.60 .002	.006	.002	1.7	1.4
(ICRH)	15	1.39	0.37 .001	.002	.001	1.4	1.2
1.6-2.0	5	2.93	0.79 .003	.008	.003	1.9	1.5
(ICRH+OH)	15	1.57	0.40 .001	.002	.001	1.5	1.2

TABLE I. Impurity concentration and Z_{eff} derived from soft X-ray analysis for the shot shown on Fig. 2. For the light impurities a model with only C or only O contribution is considered ; the results of the two cases are given together with the corresponding Z_{eff}.

These observations are confirmed by the results of an integral bolometer looking at a central chord at a toroidal location about 1 m away from the antenna (see Fig. 7). The ratio of the radiated power flux P_{rad} to the total power coupled to the plasma $P_{tot} = P'_{OH} + P_{RF}$ does not change significantly during ICRH. P'_{OH} is the reduced OH power during ICRH and P_{RF} the RF power coupled to the plasma (see section 3). The infrared thermography of various limiters (see section 4.1) also confirms that the relative part of radiated power in the power balance does not increase.

(v) Effect of mode conversion and cyclotron layer positions. Most of the experiments were performed in the mode conversion regime with a location of the mode conversion layer about 15 cm off-center towards the low field side ($X_H \gtrsim 10$ %, $B_T = 2$ T, $\omega/2\pi = 27$ MHz). This situation gives the best heating results and the lowest density increase during ICRH.

Some minority heating experiments were performed with $X_H < 1$ %. It appears that the hydrogen cyclotron layer position is not critical. The heating effects are practically not affected when the position of this layer is moved from the center to 20 cm towards the low field side. Furthermore, the heating effects are,within the error bars, identical to those obtained under the abovementioned mode conversion conditions.

3. ANTENNA LOADING AND POWER LIMITATION

The RF power fed to the antenna is given by $P_A = P_{RF} + P_{loss} = 0.5\, G_A\, V_A^2$ where the antenna input conductance $G_A \gtrsim 3.7 \times 10^{-4} R_T$ for the narrower top antenna and $G_A \gtrsim 1.4 \times 10^{-3} R_B$ for the lower antenna. V_A is the input voltage amplitude and R is the linear specific loading resistance of the antenna [11] expressed in Ω/m. The power P_{loss} represents the antenna system losses (with $R_{Tloss} = 0.35$ Ω/m and $R_{Bloss} = 0.15$ Ω/m. P_{RF} is the net power radiated in the presence of plasma.

It should be noted that the carbonization has improved the antenna coupling by allowing operation at higher densities and with broader density profiles. Fig. 8 shows the evolution of R_T and R_B versus the central line density n_{eo} for carbonized wall condition and a main limiter radius of 46 cm. The scattering of the loading values is large as they depend on the actual wall conditions. Following a fresh carbonization a progressive diminution of the loading is observed.

The coupling follows the theoretical trends : (i) for a given wall condition it increases with n_{eo} and with decreased plasma-antenna distance ; (ii) it is larger for the narrow antenna than for the broad one ; (iii) when the two antennae are operated together with a variable phase difference between their excitations, it is found that the best loading conditions occur with their currents in phase opposition ($\sim$ axisymmetric excitation) and that the loading of each antenna, in this case, is larger than for single antenna operation. The loading resistances calculated from a single pass absorption coupling code [12] show larger relative effects for the above-mentioned point (iii) and smaller for(ii). The experimental values for (i) are found to be roughly in agreement with the theoretical results when it is assumed that a density depletion is created in front of the antenna up to the main limiter radius position.

With the maximum values of R_T and R_B achieved, the antenna efficiency P_{RF}/P_A reaches 85 to 90 %. The maximum power hitherto launched without system breakdown reached 800 kW for the broad antenna and 600 kW for the narrow one. This corresponds to $|V_A|$ values of $\sim$ 30 kV and $\sim$ 37 kV, respectively. There is no significant change of loading in the case of a reversal of the B_T direction ; this indicates that a precise alignment of the electrostatic screen blades is not mandatory.

4. POWER DEPOSITION ANALYSIS

4.1. Total Power Deposited in the Plasma.

There is evidence that almost all of the RF power is actually coupled to the plasma and converted into particle kinetic energy.

(i) Limiter infrared thermography. Infrared thermography of the heads of the pump limiter (ALT-1), positioned on the L.F.S., 40° toroidally from the antennae, and of a reference limiter placed at the bottom poloidally and separated by 180 % toroidally from ALT-1, has given identical results : when the total input power P_{tot} increases from its OH level P_{OH} to the level $P_{tot} = P'_{OH} + P_{RF}$ during ICRH, the thermal load on the limiter due to convective losses P_{th} increases at least in the same proportion as P_{tot} . The ratio $[P_{th}/P_{tot}]_{ICRH}/[P_{th}/P_{OH}]_{OH}$ ranges between 0.9 and 1.3 ; plasma motion effects can be ruled out in these results. Fig. 9 shows an example of I-R thermography of the reference limiter surface [13] for a long RF pulse : the different gradients on the infrared radiation curve during the OH and ICRH parts of the shot are clearly seen. The sharp radiation increase occurring at $\sim$ 2.3 s corresponds to a major plasma disruption.

(ii) Time evolution of the energy content at RF switch-off. If at the moment of the RF switch-off t_{off}, the transport properties of the plasma do not change abruptly , the difference of the energy slope versus time at $t = t_{off}$ must be equal to the total RF power P'_{RF} effectively coupled to the plasma, i.e. $(dE/dt)_{t_{off-}} - (dE/dt)_{t_{off+}} = P'_{RF}$. As the diamagnetic loop which measures the plasma energy content E sees the total toroidal magnetic flux in the plasma, including the SOL, the difference $P_{RF} - P'_{RF}$ only corresponds to the direct RF power losses in the wall. The part of E corresponding to the RF energy deposited near the edge or in the SOL will disappear very rapidly due to the bad confinement in this region. As a result a precise measurement of P'_{RF} requires high accuracy in the display of E versus time. The diamagnetic loop data have to be corrected for the wall time constant τ_w and the time constants of the electronic processing of the signal. The value of τ_w for TEXTOR has not been measured and is estimated theoretically. When the τ_w correction is made on the diamagnetic signal (as shown in Fig. 2a), due to the uncertainty in τ_w , values varying between 0.5 and 1.0 P_{RF} can be obtained for P'_{RF} .

4.2. Central Power Density Balance.

(i) Electron power balance. The electron temperature and the density exhibit a large sawtooth activity in the $q < 1$ region. If we neglect, as usual, at the beginning of the sawtooth, the heat conduction and convective losses, the power density balance at r = o

can be written

$$3/2\ \frac{\partial}{\partial t}\ (N_{eo}KT_{eo}) \tilde{=} P_{OH} \bullet P_{RF,e} - q_{ei} - P_{rad} \qquad (1)$$

where P_{OH}, $P_{RF,e}$, q_{ei} and P_{rad} are respectively the OH, the RF power density fed to the electrons, the power density transferred to the ions by equipartition ($q_{ei} = \frac{3m_e}{m_i} NK \frac{(T_e - T_i)}{\tau_e}$) where τ_e is the electron collision time [14] and P_{rad} the radiative power losses per unit volume. We estimate $P_{OH} = V_1 B_t (\pi a_o R_o^2 q_o)^{-1}$ from the condition $q_o \tilde{=} 1$ (as confirmed by J(r) polarimetry measurements) and P_{rad} from the data for metallic impurities from soft X-ray measurements (see Table I) and Ref. [15]. The term $1.5\ \partial/\partial t(N_{eo}KT_{eo})$ is measured from the shape of T_{eo} as obtained from ECE radiometry and of N_{eo} obtained from the Abel inverted profile. Fig. 10 shows the T_{eo} and N_{eo} sawtooth display together with the central electron energy density $3/2\ N_{eo}KT_{eo}$ near the abrupt end of the ICRH pulse for the shot of Fig. 2, and Table II shows the corresponding evaluation of the different terms of Eq. (1). Note that in the OH case Eq. (1) is rather well satisfied when all the terms are replaced by their estimated values. In the ICRH case $P_{RF,e}$, which is not known, is obtained directly from Eq. (1).

As seen on Fig. 10, a sharp change in the slope of T_{eo} versus time appears at the ICRH switch-off $t = t_{off}$. If we consider that P_{OH}, q_{ei}, P_{rad} and the convective and conductive losses do not change instantaneously, then we have at $t = t_{off}$

$$-\Delta \left[\frac{3}{2}\ \frac{\partial}{\partial t}\ (N_{eo}KT_{eo})\right]_{t=t_{off}} = P_{RF,e} \qquad (2)$$

where the first term is the change in the energy density rate of increase. Eq. (2) provides a second method for the estimation of $P_{RF,e}$. A third method is also possible when using an ECE and a density signal with sawteeth oscillations filtered out. The change of slope, at $t = t_{off}$, of the mean central electron temperature also gives $P_{RF,e}$ by the relation

$$-\Delta \left[\frac{3}{2}\ \frac{\partial}{\partial t}\ (\langle N_{eo}\rangle\langle KT_{eo}\rangle)\right]_{t=t_{off}} = P_{RF,e} \qquad (3)$$

A typical comparison of the results from these three methods is found in Table II.

(ii) Ion power balance. The power density balance for the ions at r = o can be written

$$\frac{3}{2}\ \frac{\partial}{\partial t}\ (N_{io}KT_{io}) = P_{RF,i} + q_{ei} - \frac{3}{2} N_{io}KT_{io}/\tau_{E,i} \qquad (4)$$

where $P_{RF,i}$ is the RF power density directly fed to the ions and $\tau_{E,i}$ is the central ion energy confinement time, which takes into account the conductive, convective and charge exchange losses. Assuming $\tau_{E,i}$ to be dominated by the neo-classical conductive losses from the plateau regime, we have $(\tau_{E,i})_{NC} = \chi_i^{-1} \propto T_{io}^{-5/2}$. As a result, if we compare stationary conditions in OH and ICRH, we have

$$\frac{(N_{io}KT_{io}^{5/2})_{RF}}{(N_{io}KT_{io}^{5/2})_{OH}} = \frac{P_{RF,i} + (q_{ei})_{RF}}{(q_{ei})_{OH}} \qquad (5)$$

from which $P_{RF,i}$ can be determined.

	P_{OH}	q_{ei}	P_{rad}	$3/2\ \frac{\partial(N_{eo}KT_{eo})}{\partial t}$	$P_{RF,e}$ Eq.(1)	$P_{RF,e}$ Eq.(2)	$P_{RF,e}$ Eq.(3)	$P_{RF,i}$ Eq.(5)	$P_{RF,i}$ (Eq.(6)	E(kJ)	P_{tot}(kW)
OH	175	85	5	94	-	-	-	-	-	32	340
ICRH	125	81	5	150	106	173	150	61	95	42	1245

TABLE II. Values of central power densities, expressed in mW/cm^3, during the OH and ICRH parts of the shot of Fig. 2. Values for the total energy content E and the total power coupled to the plasma P_{tot} are also given.

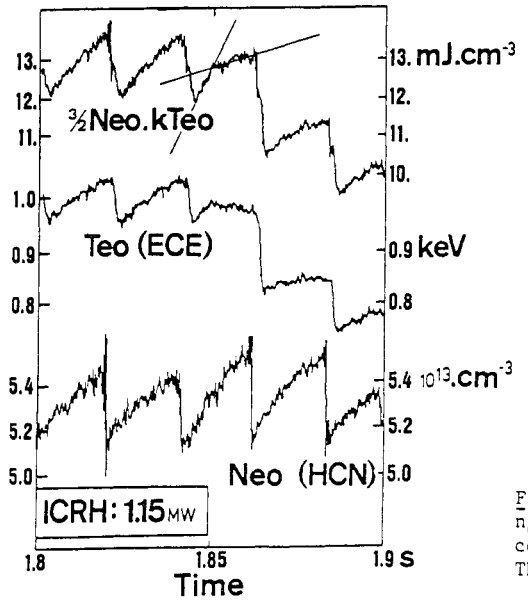

Fig. 10. Display versus time of the central temperature T_{eo}, central density N_{eo} and central energy density sawteeth around the end of the ICRH pulse (t_{off} = 1.85 s) for the shot 14169. Note the change of slope of the sawtooth at $t = t_{off}$.

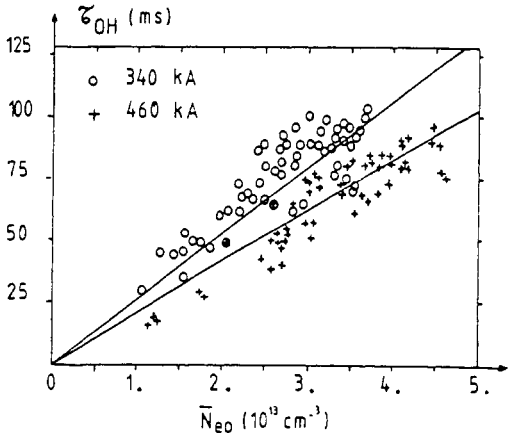

Fig. 11. Experimental points giving τ_{OH} versus $\bar{n}_{eo}$ for I_p = 340 and 460 kA. The solid lines correspond to the Neo-Alcator law given for TEXTOR in section 5.1.

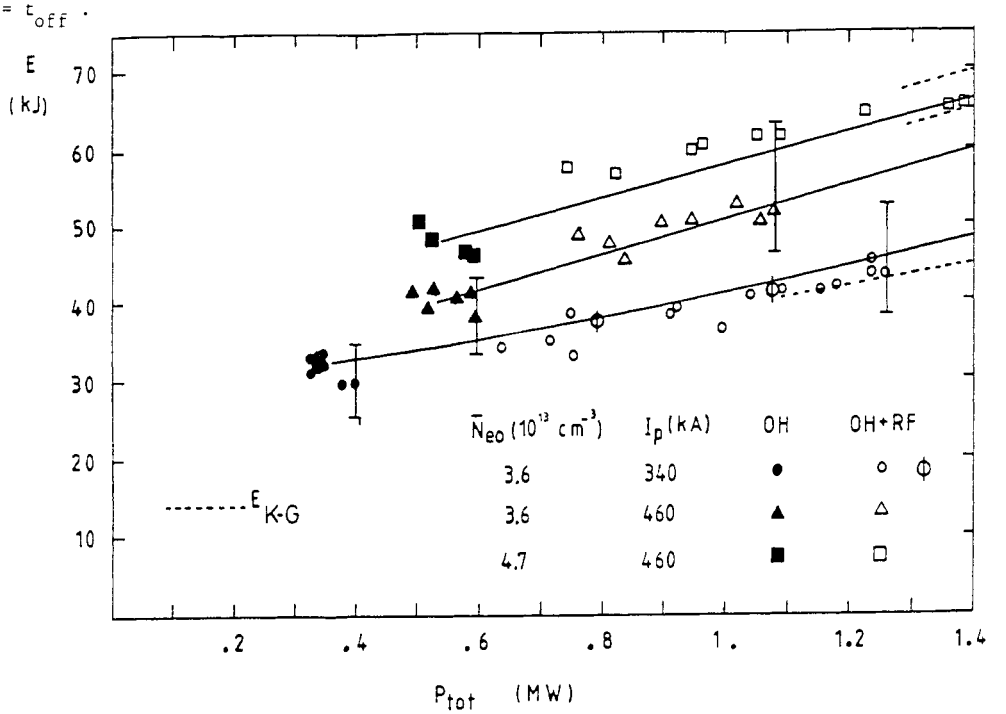

Fig. 12a. Energy content of the plasma E shown versus the total power coupled to the plasma P_{tot} at different constant central chord densities $\bar{n}_{eo}$ and currents I_p. The dotted lines display the Kaye-Goldston scaling and the solid lines the scaling using $\tau_{aux} \propto I_p$. Data corresponding to minority heating are indicated by ϕ.

$P_{RF,i}$ can be also estimated from the change of ion heating rate at the ICRH switch-off (from the decay of neutron yield). We have

$$-\Delta \left[\frac{3}{2} \frac{\partial}{\partial t} (N_{io} T_{io}) \right] = P_{RF,i} \qquad (6)$$

if we assume that $\tau_{E,i}$ and q_{ei} do not change abruptly.

Table II shows a comparison of the two estimations for $P_{RF,i}$.

It appears from this analysis that the central power deposition does not increase proportionally to the total power P_{tot} . As shown on Table II when P_{tot} is raised by a factor 3.7 the corresponding ratio of the deposited power densities($P'_{OH} + P_{RF,e} + P_{RF,i}$) is only 2. Taking these results together and the fact, as shown in 4.1, that P_{RF} is effectively coupled to the plasma, we conclude that the RF power deposition profile is broader than during the OH phase.

5. GLOBAL CONFINEMENT TIME AND ENERGY CONTENT

In this section we shall use the global confinement time $\tau_G = E/P_{tot}$, where $P_{tot} = P'_{OH} + P_{RF}$ is the total power coupled to the plasma. As defined in section 2, P'_{OH} is the ohmic power corresponding to the reduced loop voltage V'_l in presence of ICRH. From the discussion of section 4.1, we know that it is fair to assume that P_{tot} is a very good approximation to the power actually deposited in the bulk of the plasma. Such a definition of τ_G clearly is the more natural one from an engineering point of view. Note carefully that if the power deposited is actually smaller than the maximal value P_{tot}, the actual energy confinement time during ICRH will be correspondingly larger than τ_G .

5.1. OH Discharge.

In Fig. 11, from the data collected over many days of operation, we show the OH confinement time τ_{OH} as a function of density. It can be seen that TEXTOR with carbonized walls follows a Neo-Alcator law which can be expressed, from the presently available data in the range $2.5 < q_a < 6$, by the expression $\tau_{OH}(ms) \simeq 9.8\ q_a^{0.8}\ \bar{n}_{eo}(10^{13}cm^{-3})$ with a precision of ± 20% for a = 0.46 m. The resulting plasma energy content during OH is given by

$$E_{OH}(kJ) \simeq 2.9\ I_p^{0.2} \bar{n}_{eo}\ V_l \quad (kA,\ 10^{13}cm^{-3},\ V\ ;\ B_t = 2\ T) \qquad (7)$$

and for constant $\bar{n}_{eo}$ increases mainly in proportion to V_l as I_p is increased ($V_l \simeq 1.0$ or 1.2 V for I_p = 340 or 460 kA respectively).

5.2. ICRH Discharge.

Fig. 12a shows the experimentally observed increase of the energy content E when P_{tot} is raised from its OH value P_{OH} by ICRH, selecting results at constant density $\bar{n}_{eo}$ = 3.6 and 4.7 × $10^{13}cm^{-3}$ and discharge current I_p = 340 and 460 kA. From these results, it appears that : (i) at $\bar{n}_{eo}$ = 3.6 × $10^{13}cm^{-3}$, we obtain dE/dP_{tot} = 12 kJ/MW at I_p = 340 kA and dE/dP_{tot} = 21 kJ/MW at 460 kA. Both values indicate an appreciable degradation in confinement (see also Fig. 2b) but also underline the beneficial influence of the I_p increase. (ii) At constant current I_p = 460 kA, increasing $\bar{n}_{eo}$ from 3.6 to 4.7 × $10^{13}cm^{-3}$ reduces the heating rate.

It is extremely noteworthy that these low heating rates and the relative trend among them are entirely consistent with the known empirical scaling laws for auxiliary heating, the best known of which is Kaye-Goldston scaling [16]established from data of L-mode gettered neutral beam heated discharges, where the additional heating sufficiently exceeds the remaining OH power. Applying this law to TEXTOR, we expect

$$\tau_{G,K-G}(ms) = 0.021\ \bar{n}_{eo}^{0.66}\ P_{tot}^{-0.66}\ I_p^{1.04} \quad (10^{13}cm^{-3},\ MW,\ kA) \qquad (8)$$

for a = 0.46 m and B_t = 2 T when P_{tot} exceeds 3 P'_{OH} . Then , the corresponding E value reads $E_{K-G}(kJ) = 0.021\ \bar{n}_{eo}^{0.66}\ P_{tot}^{0.34}\ I_p^{1.04}$.

In Fig. 12a we have plotted E_{K-G} for the 3 cases studied in its validity range (dotted curves). It is now very clear that any smooth transition from the experimental OH values to the predicted K-G scaling can only give rise to the observed heating rates. Likewise, the density dependence of the heating rates appears as a natural consequence of a strongly

density dependent OH scaling and a practically density independent auxiliary heating scaling.

All in all, it is remarkable to what extent the present data fits the scaling, although the current dependence appears to be somewhat weaker. As Kaye-Goldston scaling describes NB experiments on clean machines, we may conclude that the observed heating efficiencies are as good as those that could be obtained on TEXTOR with NB.

The Kaye-Golston scaling is rather pessimistic because $\tau_G \propto P_{tot}^{-0.58}$ and has no non-zero asymptotic value for large values of P_{tot}, implying that the confinement degradation would go on indefinitely. It should be noted that the experimental data could be used with comparable confidence as in the K-G case, to demonstrate the existence of an asymptotic auxiliary heating confinement time $\tau_{aux} = (\Delta E)_{RF}/P_{RF}$ to which $\tau_G = E/P_{tot}$ reduces when $P_{RF} >> P'_{OH}$ In Fig. 12a we represent in solid lines the predictions corresponding to the assumption $E = E_{OH} + E_{aux} = \tau_{OH} P'_{OH} + \tau_{aux} P_{RF}$ when τ_{OH} is taken from Eq. (7) and where we use

$$\tau_{aux}(ms) = 70\ I_p(MA) \qquad (9)$$

The resulting $\tau_G = E/(P'_{OH} + P_{RF})$ is shown by the solid line in Fig. 12b. A scaling like Eq. (9) was previously proposed in [17] for τ_{aux} of D-III and in [18] for τ_G of Asdex in the H-regime.

Although our data does not allow any discrimination between the two alternatives, namely Eq. (8) or Eq. (9), they both clearly show the importance of increasing the plasma current to avoid a significant reduction of τ_G with respect to τ_{OH}. Indeed, we have $\tau_{OH} \propto I_p^{-0.8}$ and $\tau_G \propto I_p$ for $P_{RF} >> P'_{OH}$!

It is pertinent to ask whether the appreciable degradation in confinement could be explained without invoking transport degradation.

From § 5.1, we know that at best a small fraction of P_{RF} might end up directly on the walls without being converted to kinetic energy of plasma particles. Therefore, the only possible alternative to genuine degradation would be a poor energy deposition profile.

Referring to the case of Fig. 2, we observe that when P_{tot} increased from 340 to 1245 kW, the central power density increases from 0.17 W to 0.33 W/cm^3 and yet E only goes up from ~30 to ~40 kJ. Power deposition profiles capable of reconciling these figures would be ones which are both strongly peaked at the very center and at the extreme plasma edge and would be completely inconsistent with the theoretical expectations from ray-tracing.

Nevertheless, the above data also clearly indicate that the RF power deposition profile cannot be as central as the OH one and a part of the degradation is due to profile effects.

Turning to Fig. 12a, it is seen that an increase of the OH power from ~ 330 to ~ 540 kW (brought about by a current increase from 340 to 460 kA) resulted in an energy increase of 7.5 kJ, yielding an equivalent heating rate of 36 kJ/MW as opposed to 100 kJ/MW for the first 330 kW. It appears as if the OH regime also is characterized by a degradation of confinement, although it is clear that this could be partly due to a different deposition profile. Indeed, the extra 210 kW have a much broader deposition profile than the initial 330 kW since the power density in the center is expected to increase only by about 20 % due to the change in the loop voltage.

REFERENCES

[1] V.P. Bhatnagar et al., Proc. 13th Symp. on Fusion Technology (SOFT), Varese, Pergamon Press, Vol. I, 675 (1984).
[2] K.H. Dippel et al., contributed papers, this conference.
[3] TFR Group, A. Truc and D. Gresillon, Nucl. Fusion 22, 1577 (1982)
[4] R. Weynants et al., Proc. 6th Topical Conf. on RF Plasma Heating, Pine Mountain, Georgia, May 1985.
[5] G. Waidmann et al., Plasma Phys. and Contr. Nucl. Fusion Research 1984, Edit. IAEA, Nuclear Fusion Suppl., Vol. I, 193 (1985).
[6] J. Schlüter et al., contributed papers, this conference.
[7] W. Brüssau and H. Soltwisch, to be published (1985).
[8] G. Hrehuss and G. Waidmann, contributed papers, this conference.
[9] H. Soltwisch et al., Proc. invited papers Int. Conf. Plasma Phys. , Lausanne,1984, Vol. 1, 499.
[10] H.L. Bay and B. Schweer, J. Nucl. Material, 128 & 129, 257 (1984).

[11] A. Messiaen et al., "Heating in toroidal plasmas", Commission of the European Communities, Vol. I (1982) 243. Note that the loading resistance R_{TFR} defined by the TFR Group is related to G_A by $R_{TFR} = Z_f^2 G_A |V_A|^2 / |V_f|^2_{max}$ where Z_f and $|V_f|_{max}$ are respectively the feeder characteristic impedance and the maximum voltage amplitude on the feeder.
[12] R. Koch et al., Proc. 3rd European workshop on problems in plasmas, Numop 85, Varenna Sept. 1985.
[13] U. Samm, Proc. 11th Eur. Conf. on Contr. Fusion and Plasma Phys., contributed papers, Part II, 413 (1983).
[14] S.I. Braginskii, in "Reviews of Plasma Physics" Vol. 1 (edited by M. Leontovich), Consultants Bureau, New York, 1965.
[15] R.V. Jensen et al., Nuclear Fusion 17, 1187 (1977) ; D.E. Post et al., Princeton PPL Report 1352 (1977).
[16] S.M. Kaye and R.J. Goldston, Nuclear Fusion 25, 65 (1985).
[17] N. Nagami et al., Plasma Phys. and Contr. Nucl. Fusion Research, 1982, Edit. IAEA, Nuclear Fusion Suppl., Vol. I, 27 (1983).
[18] W. Köppendörfer et al., IPP Report 1/237, Max-Planck-Institut für Plasmaphysik, April 85.

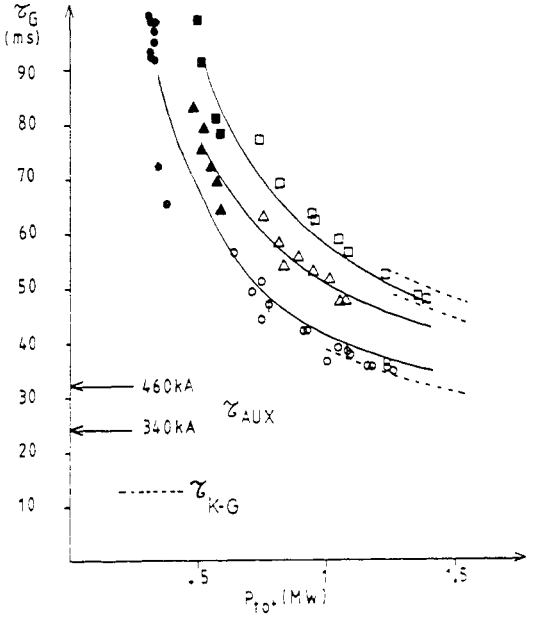

Fig. 12b. Display of the same data as in Fig. 12a) giving the global energy confinement time τ_G versus P_{tot}. The same symbols as for Fig. 12a) are used.